Physical properties controlling water repellency in synthesized granular solids

Y. SAULICK [a], S.D.N. LOURENÇO [a], B.A. BAUDET [b], S. K. WOCHE [c] & J. BACHMANN [c]

[a] *Department of Civil Engineering, Haking Wong Building, The University of Hong Kong, Pokfulam Road, Hong Kong SAR,* [b] *Department of Civil, Environmental and Geomatic Engineering, University College, London, Gower Street, London WC1E 6BT, UK, and* [c] *Institute of Soil Science, Faculty of Natural Sciences, Leibniz University Hannover, Herrenhaeuser Str.2, 30419, Hannover, Germany*

Correspondence: S.D.N. Lourenço. E-mail: lourenco@hku.hk

Running title: Synthesized water repellent granular solids

Summary

The wettability of granular solids such as soil is known to depend primarily on two factors: their inherent chemistry and their physical properties such as their particle size, particle shape and surface roughness. Nevertheless, the distinctive physical properties of such materials have not been fully explored to gauge their wettability. In this study, the difference in wettability between a flat solid (microscope slide) and three granular solids, namely: glass beads (GB), Leighton Buzzard Sand (LBS) and crushed Glass (CG) which have different physical properties were examined. The effect of chemistry was isolated by strongly hydrophobizing the above materials by treatment with dimethyldichlorosilane. Wettability measurements were made by measuring the water–solid contact angle (CA) by the sessile drop method after adhering one-layer of uniformly-oriented granular solids onto double-sided adhesive tape initially attached to a microscope slide. Techniques for particle characterization included sieving for particle size, dynamic image analysis for particle shape and confocal laser microscopy to determine surface roughness. Results show that all CAs of the granular solids exceeded that of the hydrophobized microscope slide (103°). The crushed glass had the largest CA (125°). With all three granular solids, there was an increase in CAs as particle size decreased. In addition, as particles became more

angular, CAs increased. The influence of shape on wettability became more predominant as particle size decreased. The surface roughness parameter, $R_{a,}$ was investigated and shown to be sensitive to both the size and shape of the particles. A decrease in R_a from 95.4 to 34.1 μm increased CAs from 107 to 125°. A similar change in CA was shown to correspond to an increase in void fraction from 40.7 to 77.4 %. Our results have practical implications for the optimum use of soil by enhancing or suppressing water repellency.

Keywords: wetting, contact angle, hydrophobicity

Highlights

- **How do the physical properties of granular solids such as soil influence their wettability?**
- **Effects of physical properties of particles on CAs were investigated when isolated from effect of chemistry.**
- **Particle shape becomes more important in gauging wettability as particle size decreases.**

- **Wettability of granular solids may be physically controlled by specific particle characteristics.**

Introduction

Soil water repellency is known to influence hydrological processes such as infiltration (de Jonge *et al*., 2007). A small to medium degree of water repellency in soil is important for the stability of aggregates (Hallett & Young, 1999; Goebel *et al*, 2012), but severe water repellency has been reported to lead to erosion by water (Shakesby *et al*., 2000) and wind (Ravi *et al*., 2009). The wetting properties of solids are characterized by their contact angle (CA), with a lower and upper boundary of 0° and 180° respectively. Granular solids such as soil show relatively larger CAs than flat solids. Some reported values of maximum CAs of granular solids hydrophobized by treatment with silane compounds were 126° (Bachmann & McHale, 2009), 127° (Liu *et al*., 2012) and 131° (Chan & Lourenço, 2016). McHale *et al*. (2005) also demonstrated that CAs of synthesized water repellent sand by fluorine-based compounds can reach values > 130°. In contrast, CAs of flat surfaces treated with silane-based compounds do not exceed 108° in general (Gao & McCarthy, 2006). Contact angles reported within the past decade on such surfaces were 108° (Cheng *et al*., 2014), 103° (Zhang *et al*., 2015) and can be as small as 96° (Bachmann & McHale, 2009).

Most of the literature documenting water repellency in soil revolves around the presence of organic matter (e.g. Ellies *et al*., 2005) originating from vegetation and microbial activity, which alters the chemistry of soil particles, whereas little attention has been given to decipher the role of distinct topographies of soil particles on their wettability. With soil particles, their topographies manifest themselves primarily through their size and shape. These factors (individually or combined), together with the effect of voids in between particles affect the wetting properties of granular and porous media.

Particle size has been investigated in many disciplines such as soil science and geotechnical engineering. McGhie & Posner (1980) found that coarser fractions of a sand had a larger CA than the finer fractions (a difference of up to 45°), whereas Bachmann *et al*. (2000) in their investigation of wettability of a soil from a natural soil profile observed a decrease in CAs as particles became coarser. On the other hand, Dang-Vu & Hupka (2005) investigated the effect of particle size of glass beads on wettability and showed no dependence of CAs on their size. The effect of particle shape on wettability has been examined mainly in the field of mineral engineering where the process of froth flotation is used to separate minerals, not only with respect to their particle size but also according to their shape. Lourenço *et al*. (2015) showed in their investigation of the wettability of a range of minerals, which included silicates,

carbonates, oxides and sulphides, that spherical particles and those with larger aspect ratios had larger CAs. In contrast, Ulusoy *et al*. (2003) investigated the wettability of talc particles and found that elongated and flat particles were more water repellent than rounded particles. The link between surface roughness and wettability of solids has been explored in several studies to enhance mineral recovery and to identify the range of surface roughness below which this property does not affect CAs (Chau *et al*., 2009).

The specific objectives of this study were thus to: (i) analyse the CAs of granular solids compared to a flat solid, and to relate particle size, shape and the influence of voids to differences in CAs, (ii) investigate the effect of surface roughness on water repellency and (iii) compare the experimental results with the outcomes of theoretical models such as the Wenzel model, Cassie–Baxter model and the model proposed by Bachmann & McHale (2009).

Background

Contact angle and wetting models

Young's model (Young, 1805) lies at the core of studies that make use of CA as a measure of wettability. The model describes the relation between the interfacial forces along the horizontal contact line leading to Equation (1), where θ_y is the Young's CA and γ_{sl}, γ_{sg} and γ_{lg} correspond to the interfacial forces between the solid–liquid, solid–gas and liquid–gas phases. The model is valid only for ideal surfaces and predicts a unique value of CA for a given three-phase system in thermodynamic equilibrium without considering any CA hysteresis. On real surfaces in nature such as soil, CA hysteresis is caused by chemical heterogeneity and roughness effects. Consequently, Young's model is, *sensu stricto*, not applicable because the CA value obtained experimentally is not equal to θ_y.

$$\cos\theta_y = \frac{\gamma_{sg} - \gamma_{sl}}{\gamma_{lg}}. \qquad (1)$$

Wenzel (1936) investigated the effect of roughness on surfaces and proposed to modify Young's model by a factor r_f as shown in Equation (2). This factor (r_f) is a geometric parameter that is independent of properties of the material; it is defined as the ratio of the actual area of the surface to its projected area. In this model, the drop

of liquid adheres fully to the groves of the solid as illustrated in Figure 1(a), and intensification of the Wenzel CA (θ_w) can only be achieved if θ_y is larger than 90° because $r_f \geq 1$.

$$\cos\theta_w = r_f \cos\theta_y. \quad (2)$$

To account for the inhomogeneity of solids, the Cassie model is used to predict CA, provided that θ_y of the different chemical components constituting the solids are known. The CA recorded is a weighted average of surface area of the various chemical components and their respective CA in contact with the drop of liquid.

For porous solids, such as water repellent soil, the drop of liquid can arch over different particles causing air to be trapped between the solid and liquid phase as shown in Figure 1(b). Air is the most water repellent material with a CA of 180º. The Cassie model reduces to the Cassie–Baxter model (Equation (3)) assuming that the solid particles have the same chemistry (Cassie & Baxter, 1944). The Cassie–Baxter model relates the CA (θ_{cb}) to the θ_y of the solid. This model applied to surfaces such as soil necessitates the absence of gravitational effects on the drop shape. To satisfy this condition, the gaps in between the soil particles should be less than the capillary length. The capillary length denotes a characteristic length of 2.7 mm for water at

144 standard temperature and pressure above which gravity markedly distorts the drop
145 shape. The coefficients f_1 and f_2 (equivalent to 1–f_1) refer to the fractions of the drop
146 of liquid in contact with the solid and the air respectively. As f_2, the fraction of liquid
147 in contact with the air increases, f_1 decreases, causing the magnitude of θ_{cb} to
148 approach the CA of air. For the extreme case where $f_1 = 1$, $\theta_{cb} = \theta_y$. There are
149 considerable challenges to the quantification of f_1 and f_2 because the exact way in
150 which the sessile drop advances and spreads from one particle to another is difficult to
151 determine (Chau *et al*., 2009).
152
153 $$\cos\theta_{cb} = f_1\cos\theta_y - f_2. \qquad (3)$$
154
155 The combination of the Wenzel and Cassie–Baxter models has also been applied
156 in several studies to predict CAs of a surface. Recently, Bachmann & McHale (2009)
157 derived a model based on uniform spheres where it was assumed that a drop of liquid
158 on one of the spheres completely wets a fraction of the curved surface area (Wenzel
159 model) and curls over to the adjacent sphere with air enclosed beneath (Cassie–Baxter
160 model). The model relates the predicted CA (θ_m) to θ_y by considering the packing of
161 the particles with a spacing parameter, ε, according to Equation (4). A relatively close
162 compact arrangement of particles attached to a plane and rigid surface will have a

value of ε close to 0 (i.e. a smaller liquid–air interface) than for particles with looser configurations where the liquid–air interface is considerably larger. When $\varepsilon > 0.3$, Equation (4) predicts an increase in θ_{m} for all values of θ_{y} as follows:

$$\cos\theta_{\mathrm{m}} = \frac{\pi(1+\cos\theta_{\mathrm{y}})}{\sqrt{3(1+\varepsilon)^2}}\cos\theta_{\mathrm{y}} - \left(1 - \frac{\pi\sin^2\theta_{\mathrm{y}}}{2\sqrt{3(1+\varepsilon)^2}}\right). \quad (4)$$

Particle characterization

Particle size is a fundamental property used for the characterization of granular solids. A sieve analysis is often used to determine the particle-size distribution. In comparison, the measurement of particle shape requires more subtle approaches, consequently descriptions are often qualitative such as angular, sub-angular and flaky. Semi-quantitative methods to characterize particle shape include visual comparison of particles against charts developed in the mid-twentieth century by Powers (1953). The chart uses two of the most commonly used shape parameters in the literature: sphericity and roundness. The former describes the extent to which a particle deviates from a perfect sphere and the latter is a measure of how sharp the edges of a particle are. In the chart, two different classes of sphericity and six categories of roundness are defined; values between 0.12 and 1.00 are associated with roundness. Such techniques are time consuming given the large number of particles that need to be assessed individually and can also be very user-dependent. To overcome subjectivity and improve accuracy in particle shape measurements, 2-D images may be obtained from conventional optical microscopy techniques and analysed by image-processing in packages such as ImageJ, an open source software of the National Institutes of Health (http://rsb.info.nih.gov/ij/). Although these static image analyses offer improvements

189 over visual comparisons, characterization of a large number of particles in a wide
190 range of orientations remains time consuming. In addition to the complexity of
191 characterizing particle shape, is the large number of shape parameters described in the
192 literature. These parameters often have the same connotation, but different terms are
193 used to describe them such as convexity ratio (defined as the ratio of the whole area of
194 a particle to its convex area), which was used in Mora & Kwan (2000) and has the
195 same definition as solidity used in ISO 9276-6 (International Organization for
196 Standardization ISO, 2008). In this study, the shape parameters were investigated by a
197 dynamic image analyser; they are sphericity, aspect ratio, convexity and roundness.

198 With granular solids, two scales of surface roughness are recognized, namely the
199 surface roughness of single particles as investigated by Otsubo *et al*. (2015) on glass
200 beads and surface roughness taking into consideration a series of particles as used in
201 Ulusoy *et al*. (2003). In both cases, surface roughness measures the fluctuations in
202 heights with respect to a reference line or plane. Measurements of surface roughness
203 are typically reported by statistical parameters such as centre-line averages (R_a), root
204 mean square (R_q), maximum peak height (R_p) and maximum valley depth (R_v).
205 Techniques to quantify the surface roughness include mechanical methods such as
206 atomic force microscopy and optical methods such as confocal instruments.
207 Compared to the mechanical methods, optical ones can differentiate better between

208 the edges and outlines of features that tend to give a larger magnitude of surface
209 roughness for the same area considered (Whitehouse, 2002).

210 Techniques for measuring the void fraction include 2-D quantification
211 techniques such as optical light microscopy and scanning electron microscopy.
212 Images obtained from such instruments can then be analysed by image processing
213 packages such as ImageJ following noise removal. Three-dimensional techniques to
214 quantify voids include non-destructive techniques such as X-ray computed
215 tomography and confocal instruments. These devices enable a 3-D reconstruction for
216 a given area from which a void fraction based on volume may be determined.

217 In this study, the measurement of surface roughness by R_a values and
218 quantification of the void fraction was possible by making use of a confocal laser
219 scanning microscope. Figure 2(a) depicts a schematic representation of the particle
220 characteristics defined including particle size, particle shape and surface roughness.
221

Materials and methods

Materials

Silica sand from a quarry in Leighton Buzzard, Bedfordshire, UK., and referred to as Leighton Buzzard Sand (LBS), was used. A fundamental part of this study involved investigation of the effect of particle shape on wettability. The use of artificial particles facilitates this task because they provide more control over their characterization. Glass beads (GB) and crushed Glass (CG) particles have distinctive shapes and were used to compare the effect of shape on wettability. The GB were characterized by the manufacturer according to their size (mm) as follows: <0.1, 0.2–0.4, 0.4–0.6, 0.6–0.8, 0.8–1.0, 1.0–1.5 and 1.5–2.0. To ascertain that the artificial particles had the same initial chemistry, the three largest sizes of GB were crushed with a 2.5-kg hammer in a steel mould, therefore, particles of considerably different shapes and sizes resulted. The flat solid sample base, a reference for an ideal surface, was a microscope glass slide (dimensions 76 mm by 26 mm and thickness of 1 mm), made of soda lime-silica glass because its chemistry was comparable to the granular solids (consisting predominantly of silica).

241 *Coating of solids*

242

243 The three granular solids were sieved under dry conditions with samples of materials
244 of at least 100 g; the following different particle sizes (μm) were isolated: 63–212,
245 212–300, 300–425 and 425–600. The granular solids were air-dried and all solids
246 considered were originally wettable (CA close to 0º). To alter the wettability of the
247 solids, dimethyldichlorosilane (DMDCS), an organo silicon compound (molecular
248 weight of 129.1 g mol^{-1} and density 1.06 g cm^{-3}) obtained from Acros Organics,
249 Morris Plains, NJ, USA in its liquid form was used. The reaction between the granular
250 solids and DMDCS produces a structure consisting of strong covalent siloxane bonds
251 between the silane functional group and the original surface. The reaction differs
252 considerably from coatings induced by organic substances which are more likely to be
253 abraded and thus less stable over time.

254 To minimize the effect of chemistry, i.e. insufficient coating, synthesis of the
255 granular solids was done beyond the critical concentration, which is considered the
256 smallest concentration of DMDCS required to achieve the maximum CA. Beyond this
257 concentration, no further increase in CA is possible solely by the addition of DMDCS.
258 Chan & Lourenço (2016) identified this concentration to be 0.00175% for an air-dried
259 clean sand treated with DMDCS. In this study, we added 140 μl of DMDCS from a

single channel pipette (Pipetman P100 from Gilson®, Villiers-le-Bel, France) to a 40-g sample of granular solids (10 g of each of the aforementioned particle sizes). This corresponded to a concentration of 0.37%. The microscope glass slide was made water repellent by dispensing a total volume of 20 µl of DMDCS on to its surface.

Wettability measurements

The wettability was assessed by the static contact angle, also referred to as apparent contact angle because of effects of chemical heterogeneity and roughness (Drelich, 2013). The measurements of apparent contact angle (here referred to as contact angle (CA)) were made by the sessile drop method using a goniometer (Drop Shape Analyser 25 from KRÜSS GmbH, Hamburg, Germany). A 10-µl drop of deionized water was dispensed by an automated syringe. The sample preparation technique involved sprinkling a mass of granular solids over a microscope slide to which double-sided adhesive tape had been initially attached. A 1 N-weight was then applied on the resulting lump of material such that one layer of the granular solid was obtained. The application of a load also eliminates elongated particles with their smallest dimension parallel to the microscope glass slide and ensures a more or less uniform orientation of particles. The resulting surface can be described as a quasi-plain surface with closely packed and uniformly shaped particles (Bachmann *et al*., 2000). The motion of the drop of liquid as it reached the sample was recorded by a charged-coupled device camera. For each of the solids in the study, regardless of their physical properties, the initial frame recorded after placing the drop and ending of mechanical perturbances was selected for the measurement of CA. This corresponded

to an average time of 50 ms. The CA measurements carried out within this short time lapse, limit infiltration of sessile drops to a minimum and prevent contact line movement that might change the values of the CAs (Shang *et al.*, 2008). In addition, the influence of gravity on drop shape can be disregarded because the gaps between the granular solids are less than the capillary length. The deposition of sessile drops on the particles can also lead to contact line pinning caused by the hindering effect of different types of edges in contact with the sessile drop. Pinning of the contact line is accompanied by an increase in CAs with no movement of the contact line and a constant drop base radius. After extracting the initial frame, CAs were then evaluated with the image processing technique proposed by Saulick *et al*. (2017). Ten CA measurements were made on each sample 24 hours after coating the solids, and from which the mean value and standard deviation were calculated. Measurements of the CAs were carried out at a temperature of between 22 and 24°C and a relative humidity between 60 and 70%.

298 *Dynamic image characterization of particle shape*

299

300 Particle shape was characterized with a dynamic image analyser, QicPic^{TM} (Sympatec
301 GmbH, Clausthal-Zellerfeld, Germany). The device has been used to assess the shape
302 of granular solids such as soil, in several studies e.g. Altuhafi *et al*. (2012). The
303 QicPic^{TM} enables samples of granular solids to be analysed by first dispersing them
304 by gravity: a 3-g mass was mounted on a feeding unit (VIBRI^{TM}) set at a specified
305 feed rate (15%) and allowed to fall through a gravity dispenser (GRADIS^{TM}) of height
306 50 cm and a gap width of 5 mm. A frame rate of 250 Hz was used enabling 40 000
307 2-D binary images at most to be evaluated within a couple of minutes. The resolution
308 of the lenses in the camera was 10 μm. The QicPic^{TM} generates cumulative
309 distributions of shape parameters with the images, from which a median value (50%)
310 is then obtained. It was assumed that the number of images analysed was large
311 enough so that analysis of more images would not affect the median value. The shape
312 parameters obtained are sphericity, aspect ratio and convexity. With reference to
313 Figure 2(b–d), the following conclusions about the shape parameters may be drawn: (i)
314 sphericity, given as the ratio of P_{eqpc} to P_{real}, is a 2-D parameter with values that vary
315 between 0 and 1, particles close to unity resemble a circle more, (ii) aspect ratio of a
316 particle has a lower and upper limit of 0 and 1, respectively, and (iii) amongst the

three shape parameters evaluated by QicPic^{TM}, convexity is the only one that is calculated as a direct function of area. Convexity is measured by comparing A_{real} to A_{cvx}. The plots of cumulative distributions of the shape parameters (sphericity, aspect ratio and convexity) for the 63–212 μm size of LBS are illustrated in Figure 3(a). Evaluation of the median values was considered representative of the sample. For example, a sphericity of 0.8819 (obtained with the LBS, with particle size 63–212 μm) is the sphericity of the particle below which 50% of the particles lie.

In addition to the three above shape parameters, roundness was calculated using the 2-D images generated. Roundness was defined as the ratio of average diameter of the inscribed circles at the edges of the particle to the maximum inscribed circle within the 2-D image as shown in Figure 2(e), which is similar to Wadell's (1932) definition. A sample of 20 images for LBS and CG was investigated. The corners of each of these particles were identified and circles were inserted manually to obtain roundness. The roundness values of GB were taken as 1.0.

Surface roughness and void fraction

The granular particles were fixed on a microscope slide before being examined by a 3-D confocal laser scanning microscope (CLSM: Keyence corporation, Osaka, Japan). The device consists of a microscope (VK-9710) connected to a violet laser (VK-9700) colour scanning unit. A lens with 20× magnification was used to obtain the images. Laser light intensity was set to a value of 1459 (adjustable on a scale of 0 (low light intensity) to 16 383 (high light intensity)). The image size obtained in the x–y plane was 0.716 mm by 0.537 mm (1024 × 768 pixels) corresponding to an area of approximately 0.385 mm^2 (region of interest). The resolution in the x and y direction was 0.7 µm. The resolution in the z-direction was 0.5 µm, i.e. optical sections were acquired in 0.5 µm increments in the vertical direction. After a series of sections was gathered, a 3-D reconstruction of the surface was generated to obtain the surface profile. Ten measurements were made systematically on each sieved fraction of the three granular solids. Figure 4 illustrates output images from the confocal laser scanning microscope with particles of LBS. The proprietary software within the CLSM, VK Viewer (version 2.4.0.1) enabled calculation of the two parameters of interest:

1. Surface roughness

Surface roughness is evaluated by first identifying a baseline (or reference surface) by the least squares method on the height data within the region of interest. The distance from the baseline to the height of each point is then evaluated by surface roughness parameters defined by ISO 4287 (International Organization for Standardization ISO,1997). The surface roughness parameter used with the CLSM was the mean height, R_a. The parameter is defined as the arithmetic mean of the absolute values of the height of each point within the region of interest. It is expressed mathematically according to Equation (5), where R_n is the height of each pixel with respect to the baseline and N is the total number of pixels in the region of interest. In contrast to particle shape, R_a is a direct reflection of the particles on the slide and quantifies the slide area by considering their orientations and the spacing between particles.

$$R_a = \frac{1}{N}\sum_{n=1}^{N}|R_n|. \qquad (5)$$

365 2. Void fraction

366 The integrated software within the CLSM, VK Viewer enabled the volume of
367 granular solids (v) on the slide to be calculated. The void fraction was calculated as
368 the difference between the total volume (V) and v expressed as percentage of V. To
369 obtain V, the heights of the lower and upper limits were adjusted accordingly from the
370 3-D reconstructed surface in the region of interest. The height of the lower limit was
371 set as the base of the slide. To obtain an average diameter that is representative of the
372 particles within the region of interest, Feret diameters (D) obtained from the QicPic^{TM}
373 were compared to the sieve fraction. Figure 3(b) illustrates such a comparison for the
374 LBS with the particle size of 63–212 μm. The median values (D_{50}) for the minimum,
375 mean and maximum Feret diameters defined by QicPic^{TM} were 186.3, 219.4 and
376 265.6 μm, respectively. These values indicate that the median value obtained from the
377 Feret minimum diameter was closest to the particle size obtained by the sieve analysis.
378 Similar observations have also been made with the other granular solids, regardless of
379 particle size. Therefore, to calculate V, the upper height limit (i.e. the average particle
380 diameter in the region of interest) was set to the median value of the Feret minimum
381 diameter.

382 .

Results and discussion

To investigate the effect of wettability on particle size, the particle shape was isolated by considering the different sizes of the same granular solid. Similarly, to examine the effect of particle shape on wettability, the particle size was isolated and a given particle size of the three granular solids was investigated.

Wettability and particle size

The mean CAs of the granular solids all exceeded the CA of the flat hydrophobized microscope slide, which was 103° (SD = 2°). The standard deviations of the CAs were 5° at most and accord with previous studies such as by Bachmann *et al*. (2000). The effect of particle size on the CAs is illustrated in Figure 5(a). The largest CA recorded (125° (SD = 4°)) was obtained with the 63–212 µm fraction of CG and the smallest one (107° (SD = 5°)) was obtained with the 425–600 µm fraction of LBS. With all three granular solids, there was a general decrease in CAs as the particle size increased. For example, with particle sizes of 63–212, 212–300, 300–425 and 425–600 µm for CG the CAs obtained are: 125° (SD = 4°), 119° (SD = 5°), 114° (SD = 4°) and 110° (SD = 5°). The difference in CAs between the extreme particle sizes (63–212 and 425–600 µm) for CG, LBS and GB are 14°, 16° and 9°, respectively.

Reasons for the larger CAs of the finer particles include a relatively larger void fraction with such particles. The plot of void fraction against particle size is shown in Figure 5(b). The smallest void fraction (37.0%) was obtained with the particle size of 425–600 μm of LBS, whereas the void fraction recorded with the particle sizes of 300–425, 212–300 and 63–212 μm of LBS were 52.0, 62.1 and 68.8%, respectively. Similar trends were also observed with the particles of GB and CG.

Wettability and particle shape

The results of the effect of particle shape for the different particle sizes of the three granular solids are shown in Figure 6. All the shape parameters considered are sensitive to the different granular solids. Of these parameters, convexity had the smallest range (from 0.8944 with the 63–212 µm particle size of CG to 0.9777 with the 425–600 µm particle size of GB), whereas the roundness showed the largest range (from 0.3046 with the 425–600 µm particle size of CG to unity with the particles of GB). The largest values of sphericity (0.9429), aspect ratio (0.9633) and convexity (0.9777) were all for GB with a particle size of 425–600 µm and the smallest values of sphericity (0.8322), aspect ratio (0.6656), convexity (0.8944) and roundness (0.3046) were obtained with CG. With the exception of convexity, the variation in particle shape across the range of particle sizes shows little to no change compared to the variation in relation to the different materials where the difference was noticeably more pronounced. The largest standard deviation of the shape parameters was for the aspect ratio of CG (0.13). This is partly attributed to the crushing process; nevertheless most standard deviations of the shape parameters of the three granular solids were comparable, for example those of sphericity for CG, LBS and GB are 0.06, 0.06 and 0.04 respectively for the particle size of 425–600 µm. Comparison of particle shape before and after reaction with DMDCS showed no change, indicating

that the thickness of the coating induced by DMDCS at a concentration of 0.37% was smaller than the resolution of the lenses in QicPic^{TM}.

Although the general trend of the shape parameters is for one of them to increase as the other increases, the extent to which they are positively correlated varies. Analysis of the shape parameters showed a relatively poor linear correlation (determined by the correlation coefficient r) between convexity and the remaining three shape parameters. The values of the correlations between convexity and roundness, sphericity and aspect ratio were 0.612, 0.743 and 0.748, respectively. Results reported by Altuhafi *et al*. (2012) showed an even weaker correlation between convexity and aspect ratio (r = 0.469). By comparison, the linear correlations between sphericity, aspect ratio and roundness were much stronger (r > 0.96). A strong correlation was noted between roundness and aspect ratio (r = 0.969) despite the difference in sample size.

Figure 7 shows the plot of contact angle against the four shape parameters. There is a reduction in CA with an increase in the value of the shape parameters. For example, for the particle-size range of 63–212 μm, a change in CA from 125° (SD = 4°) to 117° (SD = 4°) corresponded to an increase from 0.8369 to 0.9374, 0.6656 to 0.9263, 0.8944 to 0.9426 and 0.4747 to 1 in sphericity, aspect ratio, convexity and roundness, respectively. The relatively steeper slopes for the finest fractions show that

as particle size decreases, the effect of particle shape becomes more predominant in dictating wettability. Qualitatively, the angular particles were the most water repellent. These results can be attributed to pinning effects caused by the edges of particles in contact with the sessile drop. For sharp edges like those present with CG, the sessile drop adheres and becomes pinned to the edge rather than moving over it. The process of pinning with the sharp edges causes CAs to increase, as observed by Oliver *et al*. (1977). As a result, a larger force is required for the sessile drop to move to the next particle. This force can be in the form of a capillary force, which prevents the sessile drop from entering the grooves of the granular solids and increases the fraction of air between the solid and liquid interface (Cao *et al*., 2007). In contrast, with the relatively smoother edges of GB, the pinning effect was less significant resulting in a smaller CA.

Wettability and surface roughness

The relation between surface roughness, characterized by R_a on the CAs is illustrated in Figure 8. For all three granular solids, the particle-size range of 425–600 μm has the largest R_a value and it is smallest for the range 63–212 μm. Figure 8 also shows the increase in standard deviation of R_a as particle size increases: with CG, the standard deviation for the particle sizes 63–212, 212–300, 300–425 and 425–600 μm are 5.36, 8.65, 10.97 and 26.65 μm, respectively. Comparison of R_a values for the different materials shows that particles with a small shape parameter as for CG (sphericity = 0.8369, aspect ratio = 0.6656, convexity = 0.8944 and roundness = 0.4647 for particle size 63–212 μm) generally, results in a smaller R_a. For the finest particle size, the R_a values of CG, LBS and GB are as follows: 34.1 μm (SD = 5.36 μm), 44.8 μm (SD = 2.07 μm) and 58.9 μm (SD = 3.42 μm). These data show that R_a is not only sensitive to changes in particle size but also to particle shape. A fine particle size with a small shape parameter corresponds to a small value of R_a. An increase in surface roughness from 34.1 to 95.4 μm corresponds to a decrease in CA from 125 to 107°. There seems to be little to no change in CAs of the granular solids considered beyond an R_a value of 95.4 μm.

Comparison with wetting models

To investigate differences between measured CAs and theoretical models for the flat and granular solids, the measurements of CAs, surface roughness and void fractions were compared with predicted values.

The values of the roughness factor, r_f, Equation (2) for θ_y of 103° is given in Table 1. The roughness factor increases as particle size decreases; the smallest value was 1.304 obtained with the 425–600 μm particle size of LBS and the largest value was 2.531 obtained with the 63–212 μm particle size of CG. Although the values of R_a measured in this study with CLSM cannot be translated directly to a roughness factor, the increase in surface roughness leading to a decrease in CAs for the water repellent granular solids in this study qualitatively contradict the Wenzel equation.

The variation in void fraction of the granular solids with the CAs is shown in Figure 9. The largest void fraction is generally associated with the finest sieve fraction. There was a maximum difference in void fraction of around 40.4% between the particle size of 212–300 μm for CG and that of 425–600 μm for LBS. Figure 9 shows that an increase in void fraction corresponds to an increase in CA. Figure 9 also shows the Cassie–Baxter model (Equation (3)) plotted with θ_y of 103°. This model, which fails to take into account the physical properties of granular solids (particle size,

500 particle shape and their distributions) overestimates the data obtained experimentally.
501 This comparison was made with the assumption that for very water repellent granular
502 solids as used in this study, the bottom interface of the sessile drop bridges from one
503 particle to another in the case of maximum void fraction leading to additional liquid–
504 air interfaces adjacent to the solid–liquid interfaces. This effect increases the
505 measured CAs.

506 The experimental data obtained for GB were also compared with the model
507 proposed by Bachmann & McHale (2009). The explicit determination of the spacing
508 parameter, ε, using the 2-D images from CLSM gave an average value of 0.261 for
509 the particle sizes of 63–212 and 212–300 μm. This value is smaller than 0.319, the
510 value obtained by Bachmann & McHale (2009) with GB particles, but it is close to
511 the lower boundary of the stable range (0.260 to 0.320) reported by the same authors.
512 Because of difficulties in obtaining the exact location of the centroid of the LBS and
513 CG for all particle sizes, the analysis could not be done on these particles. Figure 10
514 shows the predicted contact angle by the model (θ_m) plotted against θ_y for ε equal
515 to 0.261. For $\theta_y > 42°$, the model predicts an increase in CA. The predicted CA, θ_m,
516 for $\theta_y = 103°$ is 131°. This value exceeds the maximum CA reported for GB in this
517 study (117° (SD = 4°)) which was recorded for the 63–212 μm fraction. The model is
518 very dependent on the void fraction, determined by the spacing parameter. A probable

519 reason for the overestimation of CA is because of the relatively closer and compact
520 arrangement of the particles used in this study. Figure 10 also shows the plot of ε
521 equal to 0 and 0.060, values adjusted to fit the maximum CA measured with GB,
522 taking into consideration the range of experimental error. The θ_{m} value for ε equal to
523 0 and 0.060 were 117° and 121°, respectively.
524

Conclusions

All granular solids had larger CAs than the microscope slide. Finer particle sizes had larger CAs than their coarser counterparts, irrespective of the material considered. By isolating the different sieve fractions, we showed that angular particles represented by relatively smaller values (i.e. values diverging from unity) of sphericity, aspect ratio, convexity and roundness had the largest CAs. The surface roughness, R_a, had small values for finer particle sizes and more angular particles.

Changes in CAs of granular solids have often been attributed exclusively to a change in chemistry. In this study, we assumed that the coatings were similar for all size classes and materials because the surfaces were treated with larger amounts of DMDCS than required to achieve the maximum CA. This study has shown that granular solids with a particular size and shape are able to control their wettability. Rather than relying on coatings, taking the topography of granular solids into consideration can lead to (i) reduction in the amount of chemicals (e.g. silanes) used to achieve the desired level of water repellency, (ii) a longer durability in water repellency compared to coatings that may be abraded over time and (iii) help to source suitable granular solids from natural soils and waste materials for use in applications such as slope covers.

Acknowledgements

The first author thanks The University of Hong Kong (HKU) for the Postgraduate Scholarship. Financial support provided by the General Research Fund, Research Grants Council, Hong Kong (17221016 and 17203417) and HKU seed funds for basic research (201406159004 and 201511159205) are acknowledged.

551 **References**

552

553 Altuhafi, F., O'sullivan, C. & Cavarretta, I. 2012. Analysis of an image-based method
554 to quantify the size and shape of sand particles. *Journal of Geotechnical and*
555 *Geoenvironmental Engineering*, **139,** 1290–1307.

556 Bachmann, J., Horton, R., van Der Ploeg, R.R. & Woche, S.K. 2000. Modified sessile
557 drop method for assessing initial soil-water contact angle of sandy soil. *Soil Science*
558 *Society of America Journal*, **64,** 564–567.

559 Bachmann, J. & McHale, G. 2009. Superhydrophobic surfaces: a model approach to
560 predict contact angle and surface energy of soil particles. *European Journal of Soil*
561 *Science*, **60,** 420–430.

562 Cao, L., Hu, H.-H. & Gao, D. 2007. Design and fabrication of micro-textures for
563 inducing a superhydrophobic behavior on hydrophilic materials. *Langmuir*, **23,** 4310–
564 4314.

565 Cassie, A.B.D. & Baxter, S. 1944. Wettability of porous surfaces. *Transactions of the*
566 *Faraday Society*, **40,** 546–551.

567 Chan, C.S.H. & Lourenço, S.D.N. 2016. Comparison of three silane compounds to
568 impart water repellency in an industrial sand. *Géotechnique Letters*, **6,** 263–266.

569 Chau, T.T., Bruckard, W.J., Koh, P.T.L. & Nguyen, A.V. 2009. A review of factors
570 that affect contact angle and implications for flotation practice. *Advances in Colloid*
571 *and Interface Science*, **150,** 106–115.
572 Cheng, L., Liu, Q., Lei, Y., Lin, Y. & Zhang, A. 2014. The synthesis and
573 characterization of carboxybetaine functionalized polysiloxanes for the preparation of
574 anti-fouling surfaces. *RSC Advances*, **4,** 54372–54381.
575 Dang-Vu, T. & Hupka, J. 2005. Characterization of porous materials by capillary rise
576 method. *Physicochemical problems of mineral processing*, **39,** 47–65.
577 de Jonge, L.W., Moldrup, P. & Jacobsen, O.H. 2007. Soil-water content dependency
578 of water repellency in soils. *Soil Science*, **172,** 577–588.
579 Drelich, J. 2013. Guidelines to measurements of reproducible contact angles using a
580 sessile-drop technique. *Surface Innovations*, **1,** 248–254.
581 Ellies, A., Ramírez, C. & Mac Donald, R. 2005. Organic matter and wetting capacity
582 distribution in aggregates of Chilean soils. *Catena*, **59,** 69–78.
583 Gao, L. & McCarthy, T.J. 2006. A perfectly hydrophobic surface (θA/θR= 180/180).
584 *Journal of the American Chemical Society*, **128,** 9052–9053.
585 Goebel, M.O., Woche, S.K. & Bachmann, J. 2012. Quantitative analysis of liquid
586 penetration kinetics and slaking of aggregates as related to solid–liquid interfacial
587 properties. *Journal of Hydrology*, **442,** 63–74.

588 Hallett, P.D. & Young, I.M. 1999. Changes to water repellence of soil aggregates
589 caused by substrate-induced microbial activity. *European Journal of Soil Science*, **50,**
590 35–40.
591 International Organization for Standardization ISO 1997. *Geometrical Product*
592 *Specifications (GPS)—Surface Texture: Profile Method—Terms, Definitions and*
593 *Surface Texture Parameters.* Protocol ISO 4287, International Organization for
594 Standardization, Geneva.
595 International Organization for Standardization ISO 2008. *Representation of Results of*
596 *Particle Size Analysis—Part 6: Descriptive and Quantitative Representation of*
597 *Particle Shape and Morphology.* Protocol ISO 9276-6, International Organization for
598 Standardization, Geneva.
599 Liu, H., Ju, Z., Bachmann, J., Horton, R. & Ren, T. 2012. Moisture-dependent
600 wettability of artificial hydrophobic soils and its relevance for soil water desorption
601 curves. *Soil Science Society of America Journal*, **76,** 342–349.
602 Lourenço, S.D.N., Woche, S.K., Bachmann, J. & Saulick, Y. 2015. Wettability of
603 crushed air-dried minerals. *Géotechnique Letters*, **5,** 173–177.
604 McGhie, D.A. & Posner, A.M. 1980. Water repellence of a heavy textured Western
605 Australian surface soil. *Soil Research*, **18,** 309–323.

McHale, G., Newton, M.I. & Shirtcliffe, N.J. 2005. Water-repellent soil and its relationship to granularity, surface roughness and hydrophobicity: a materials science view. *European Journal of Soil Science*, **56,** 445–452.

Mora, C.F. & Kwan, A.K.H. 2000. Sphericity, shape factor, and convexity measurement of coarse aggregate for concrete using digital image processing. *Cement and Concrete Research*, **30,** 351–358.

Oliver, J.F., Huh, C. & Mason, S.G. 1977. Resistance to spreading of liquids by sharp edges. *Journal of Colloid and Interface Science*, **59,** 568–581.

Otsubo, M., O'sullivan, C., Sim, W.W. & Ibraim, E. 2015. Quantitative assessment of the influence of surface roughness on soil stiffness. *Geotechnique*, **65,** 694–700.

Powers, M.C. 1953. A new roundness scale for sedimentary particles. *Journal of Sedimentary Research*, **23**.

Ravi, S., D'Odorico, P., Zobeck, T.M. & Over, T.M. 2009. The effect of fire-induced soil hydrophobicity on wind erosion in a semiarid grassland: experimental observations and theoretical framework. *Geomorphology*, **105,** 80–86.

Saulick, Y., Lourenço, S.D.N. & Baudet, B.A. 2017. A semi-automated technique for repeatable and reproducible contact angle measurements in granular materials using the sessile drop method. *Soil Science Society of America Journal*, **81,** 241–249.

624 Shakesby, R.A., Doerr, S.H. & Walsh, R.P.D. 2000. The erosional impact of soil
625 hydrophobicity: current problems and future research directions. *Journal of*
626 *Hydrology*, **231,** 178–191.
627 Shang, J., Flury, M., Harsh, J.B. & Zollars, R.L. 2008. Comparison of different
628 methods to measure contact angles of soil colloids. *Journal of Colloid and Interface*
629 *Science*, **328,** 299–307.
630 Ulusoy, U., Yekeler, M. & Hiçyılmaz, C. 2003. Determination of the shape,
631 morphological and wettability properties of quartz and their correlations. *Minerals*
632 *Engineering*, **16,** 951–964.
633 Wadell, H. 1932. Volume, shape, and roundness of rock particles. *The Journal of*
634 *Geology*, **40,** 443–451.
635 Wenzel, R.N. 1936. Resistance of solid surfaces to wetting by water. *Industrial &*
636 *Engineering Chemistry*, **28,** 988–994.
637 Whitehouse, D.J. 2002. *Surfaces and their Measurement*. Hermes Penton Science,
638 London.
639 Young, T. 1805. An essay on the cohesion of fluids. *Philosophical Transactions of*
640 *the Royal Society of London*, **95,** 65–87.

641 Zhang, A., Cheng, L., Hong, S., Yang, C. & Lin, Y. 2015. Preparation of anti-fouling
642 silicone elastomers by covalent immobilization of carboxybetaine. *RSC Advances*, **5,**
643 88456–88463.

644 ---

FIGURE CAPTIONS

Figure 1 Schematic illustrations of a drop of liquid in (a) Wenzel state (b) Cassie–Baxter state.

Figure 2 (a) Characterization of particles: particle size, particle shape and surface roughness characterized by sieve analysis, dynamic image analyser and confocal laser scanning microscope respectively, and (b–e) definitions of shape parameters used: sphericity, aspect ratio, convexity and roundness.

Figure 3 (a) Cumulative distribution of particle shape parameters of Leighton Buzzard Sand and evaluation of their median values and (b) particle-size distributions of Leighton Buzzard Sand.

Figure 4 Topographic images of Leighton Buzzard Sand from confocal laser scanning microscope (a) 2-D laser image, (b) 2-D height image and (c) 3-D display.

Figure 5 (a) Contact angle plotted against particle size. The error bars indicate standard error of the mean (ten measurements) and (b) variation of void fraction with particle size. The lines are to guide the eye**.**

Figure 6 Variation of (a) sphericity, (b) aspect ratio, (c) convexity and (d) roundness for the different particle sizes of the granular solids. The lines are to guide the eye. GB, Glass beads; LBS, Leighton Buzzard Sand; CG, Crushed glass.

Figure 7 Contact angle plotted against (a) sphericity, (b) aspect ratio, (c) convexity and (d) roundness. The error bars indicate standard error of the mean (ten measurements). The lines are to guide the eye.

Figure 8 Contact angle plotted against surface roughness, R_a. The error bars indicate standard error of the mean (ten measurements).

Figure 9 Variation in void fraction with contact angle

Figure 10 Predicted contact angles according to model proposed by Bachmann & McHale (2009) for the experimentally measured value of $\varepsilon = 0.261$ and fitted values of $\varepsilon = 0$ and $\varepsilon = 0.060$

TABLES

Table 1 Calculated Wenzel roughness factor, r_f from θ_y

Particle Size/μm	Granular Solids		
	GB	LBS	CG
63–212	2.004	2.428	2.531
212–300	1.981	2.244	2.173
300–425	1.580	1.592	1.783
425–600	1.378	1.304	1.543

GB, Glass beads; LBS, Leighton Buzzard Sand; CG, Crushed glass.

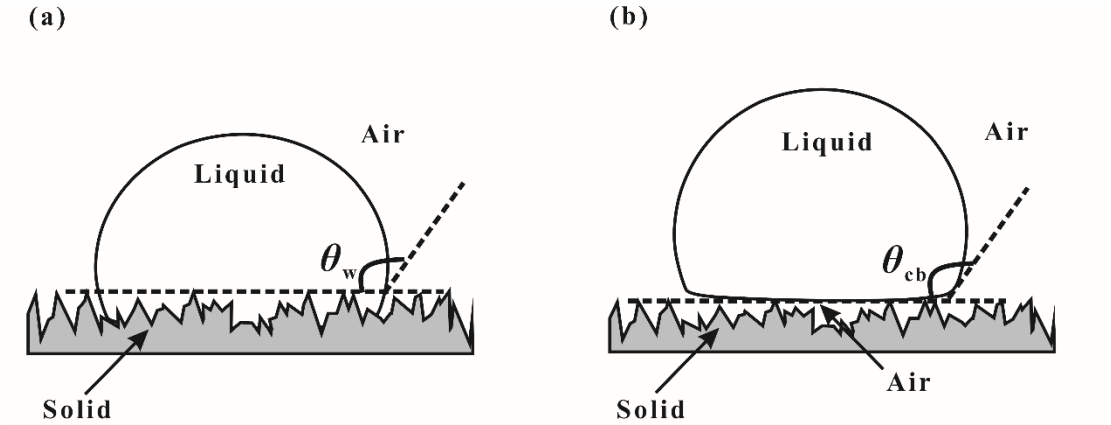

678

679 **Figure 1** Schematic illustrations of a drop of liquid in (a) Wenzel state (b) Cassie–

680 Baxter state.

681

682

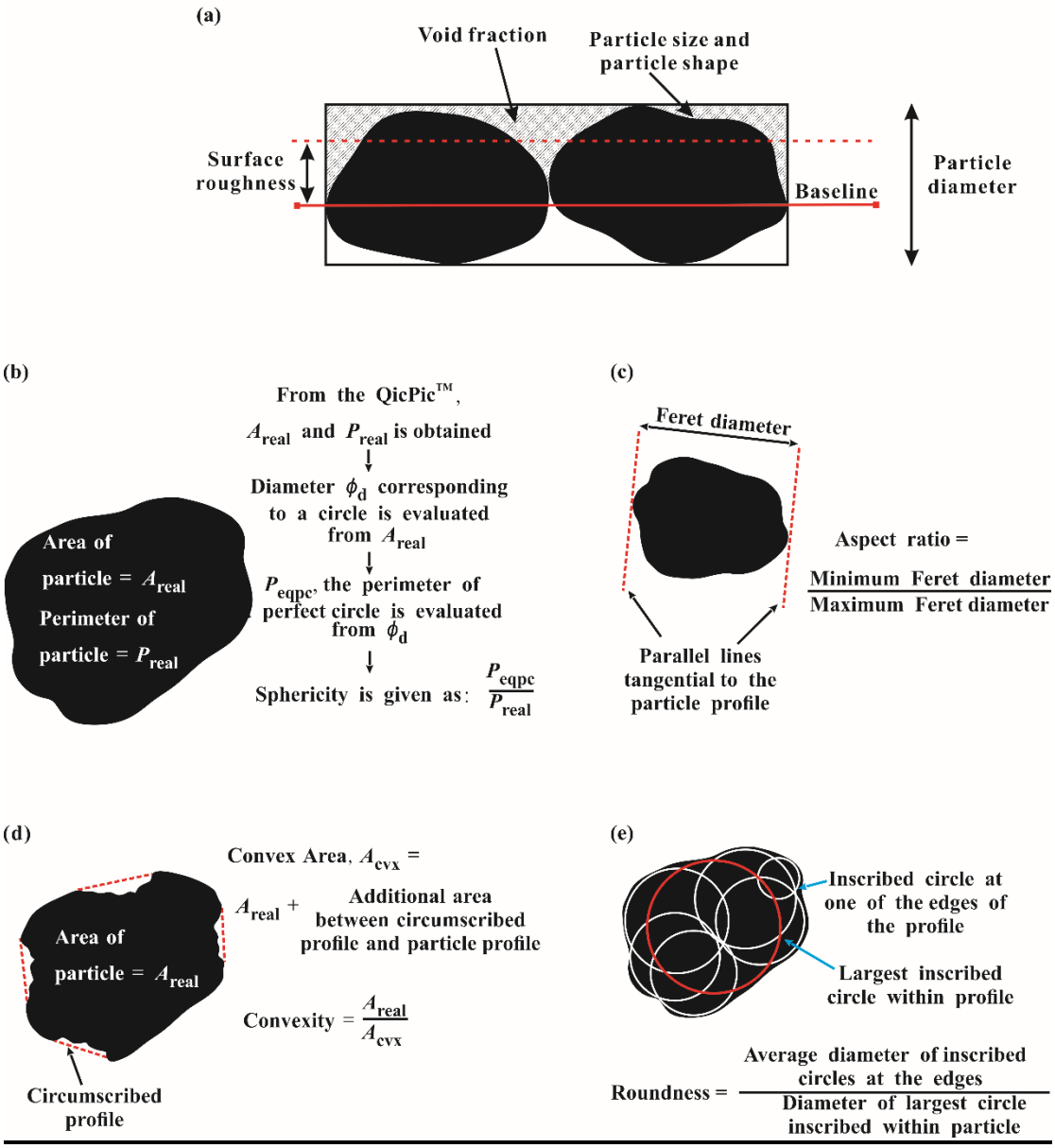

Figure 2 (a) Characterization of particles: particle size, particle shape and surface roughness characterized by sieve analysis, dynamic image analyser and confocal laser scanning microscope respectively, and (b–e) definitions of shape parameters used: sphericity, aspect ratio, convexity and roundness.

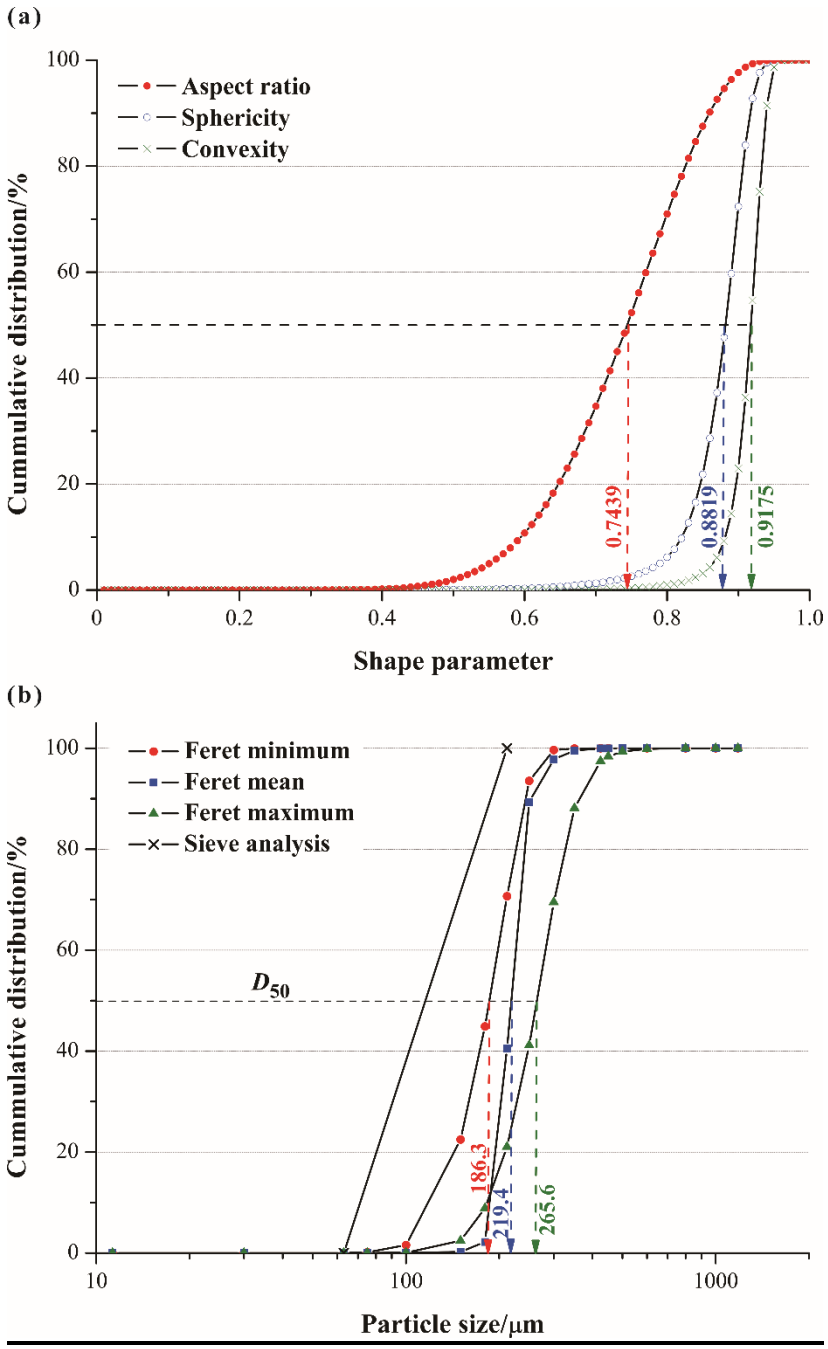

690

691 **Figure 3** (a) Cumulative distribution of particle shape parameters of Leighton

692 Buzzard Sand and evaluation of their median values and (b) particle-size distributions

693 of Leighton Buzzard Sand.

694

695

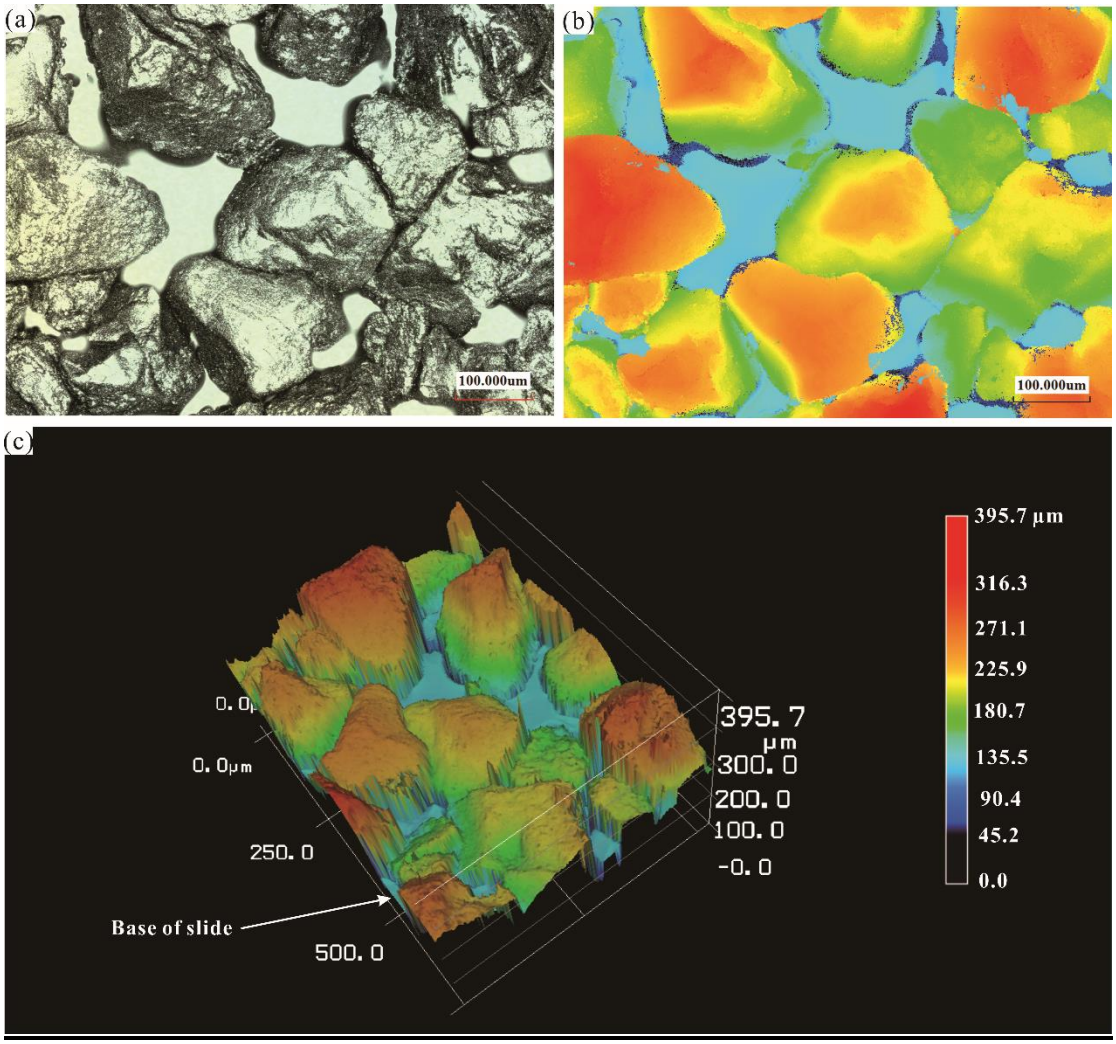

696

697 **Figure 4** Topographic images of Leighton Buzzard Sand from confocal laser

698 scanning microscope (a) 2-D laser image, (b) 2-D height image and (c) 3-D display.

699

700

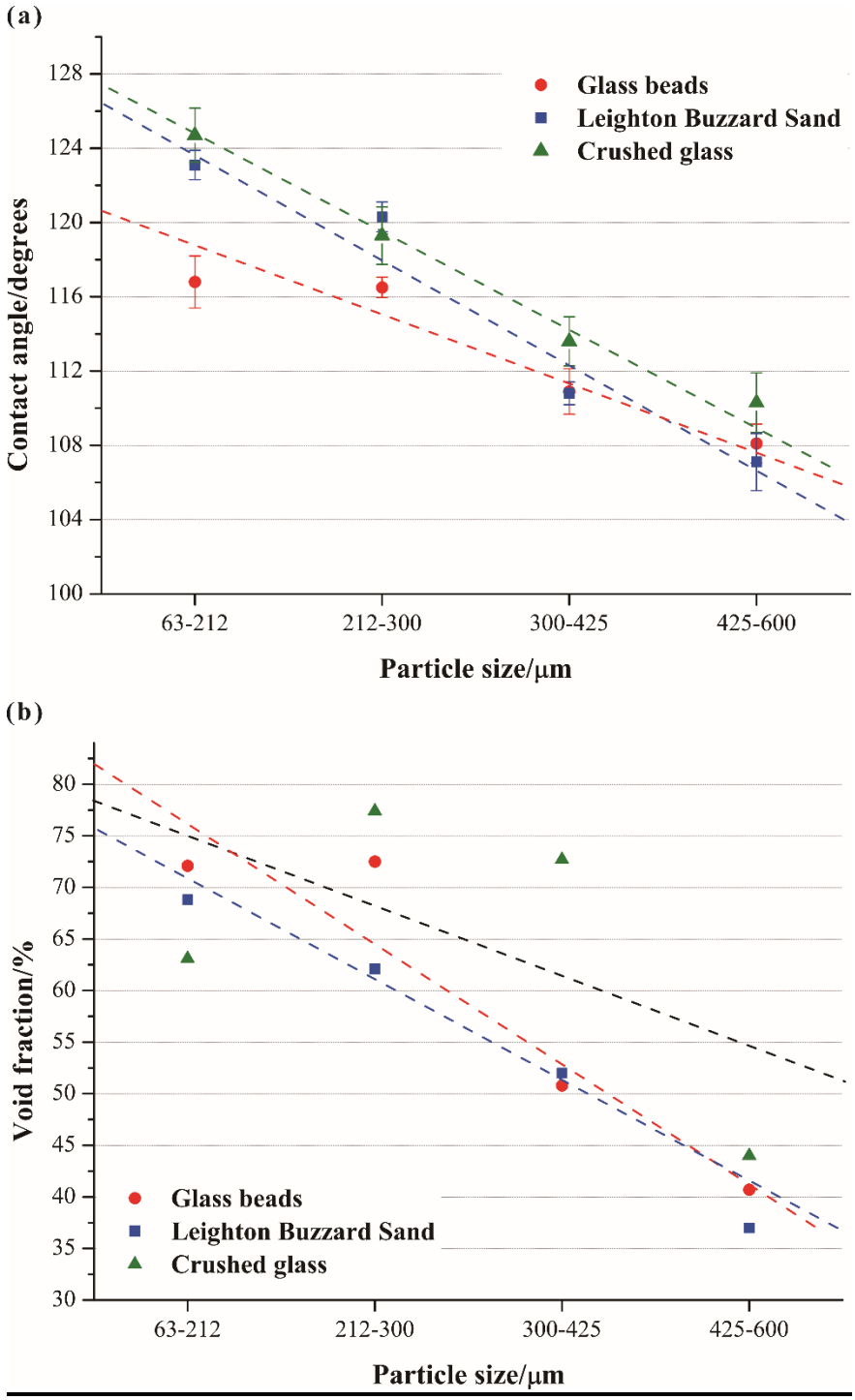

701

702 **Figure 5** (a) Contact angle plotted against particle size. The error bars indicate

703 standard error of the mean (ten measurements) and (b) variation of void fraction with

704 particle size. The lines are to guide the eye**.**

705

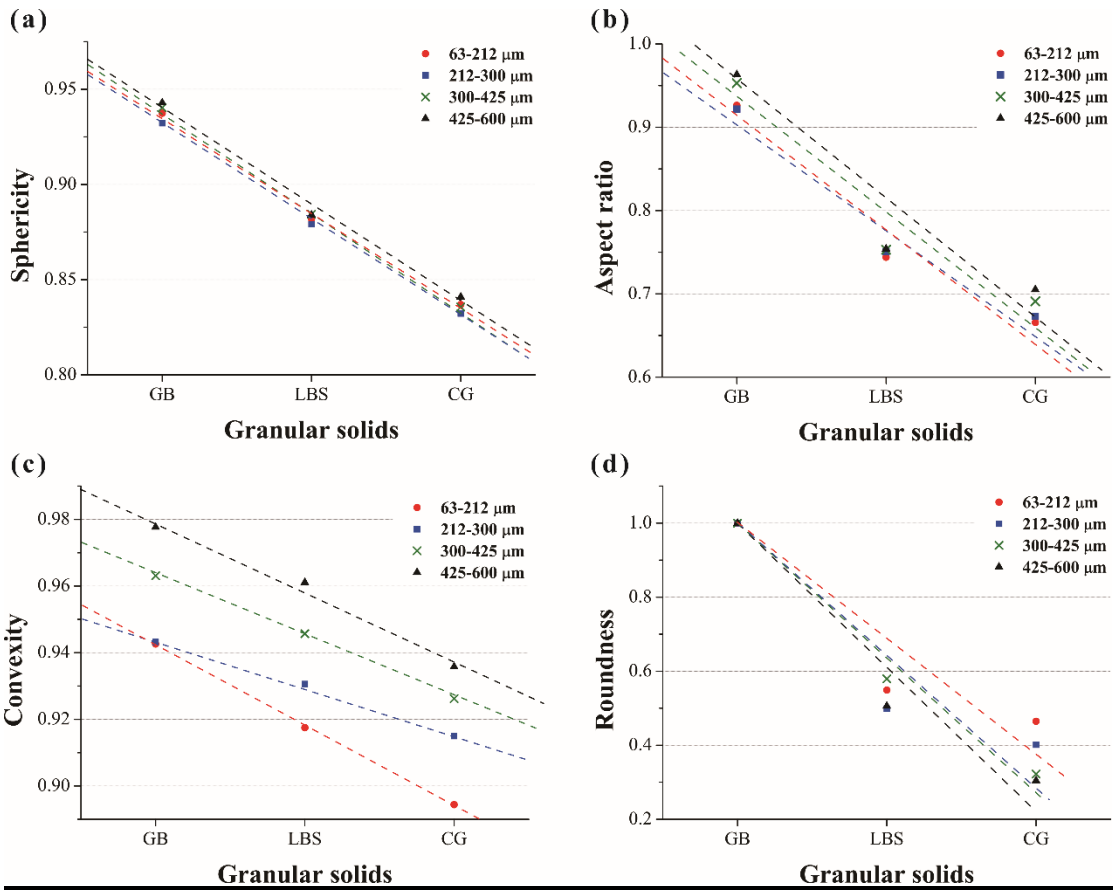

706

707 **Figure 6** Variation of (a) sphericity, (b) aspect ratio, (c) convexity and (d) roundness

708 for the different particle sizes of the granular solids. GB, LBS and CG are

709 abbreviations for Glass beads, Leighton Buzzard Sand and Crushed glass respectively.

710 The lines are to guide the eye.

711

712

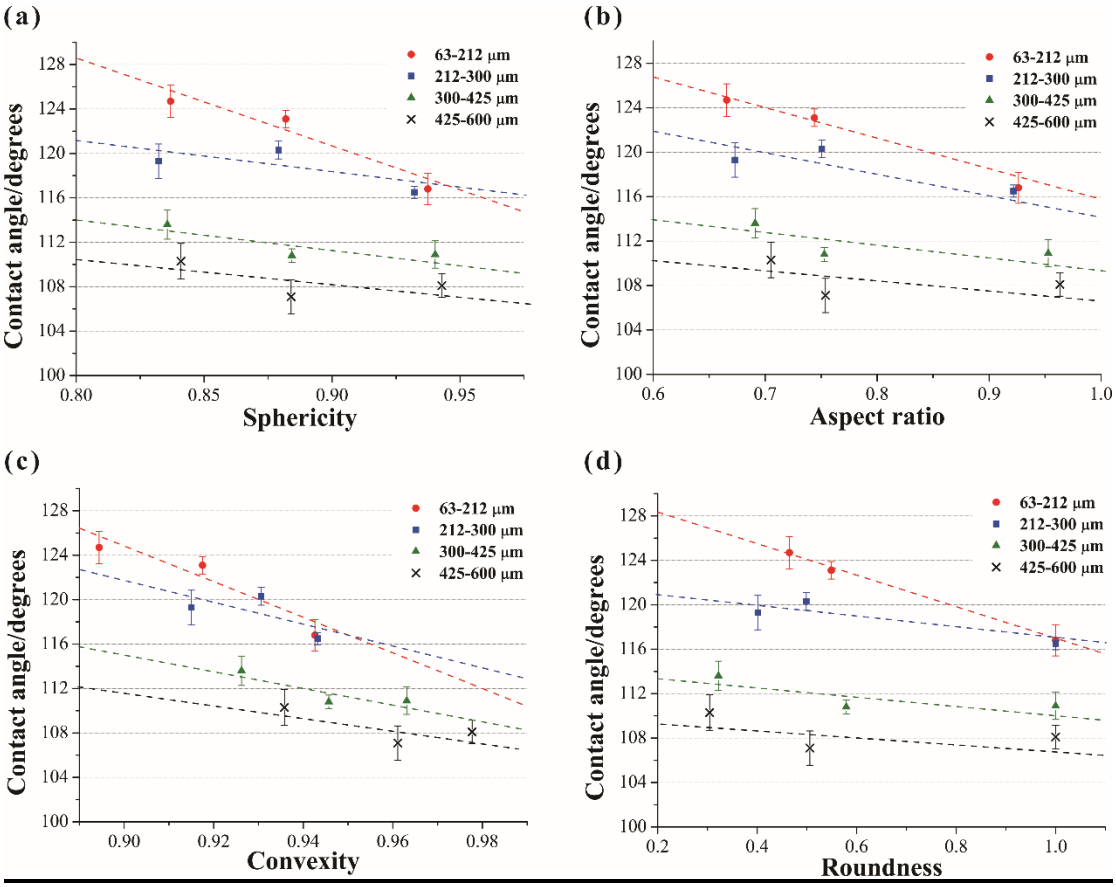

Figure 7 Contact angle plotted against (a) sphericity, (b) aspect ratio, (c) convexity and (d) roundness. The error bars indicate standard error of the mean (ten measurements). The lines are to guide the eye.

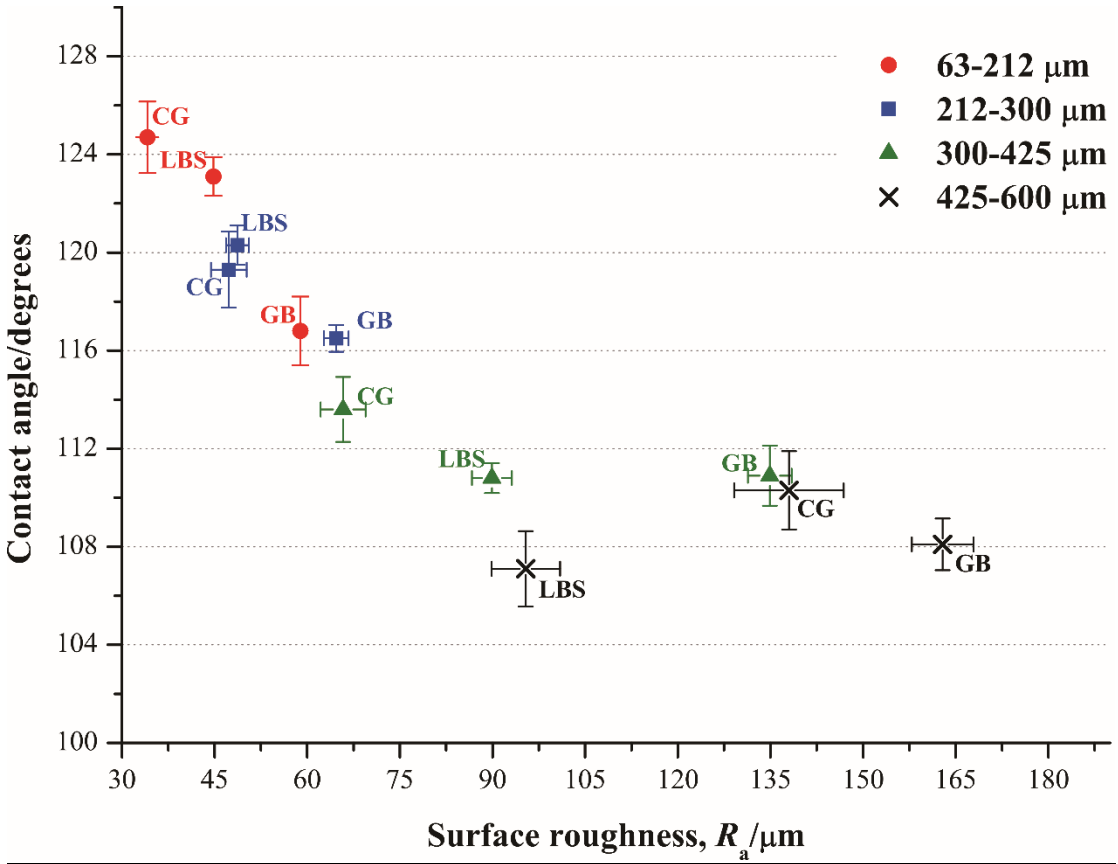

719

720 **Figure 8** Contact angle plotted against surface roughness, R_a. The error bars indicate

721 standard error of the mean (ten measurements).

722

723

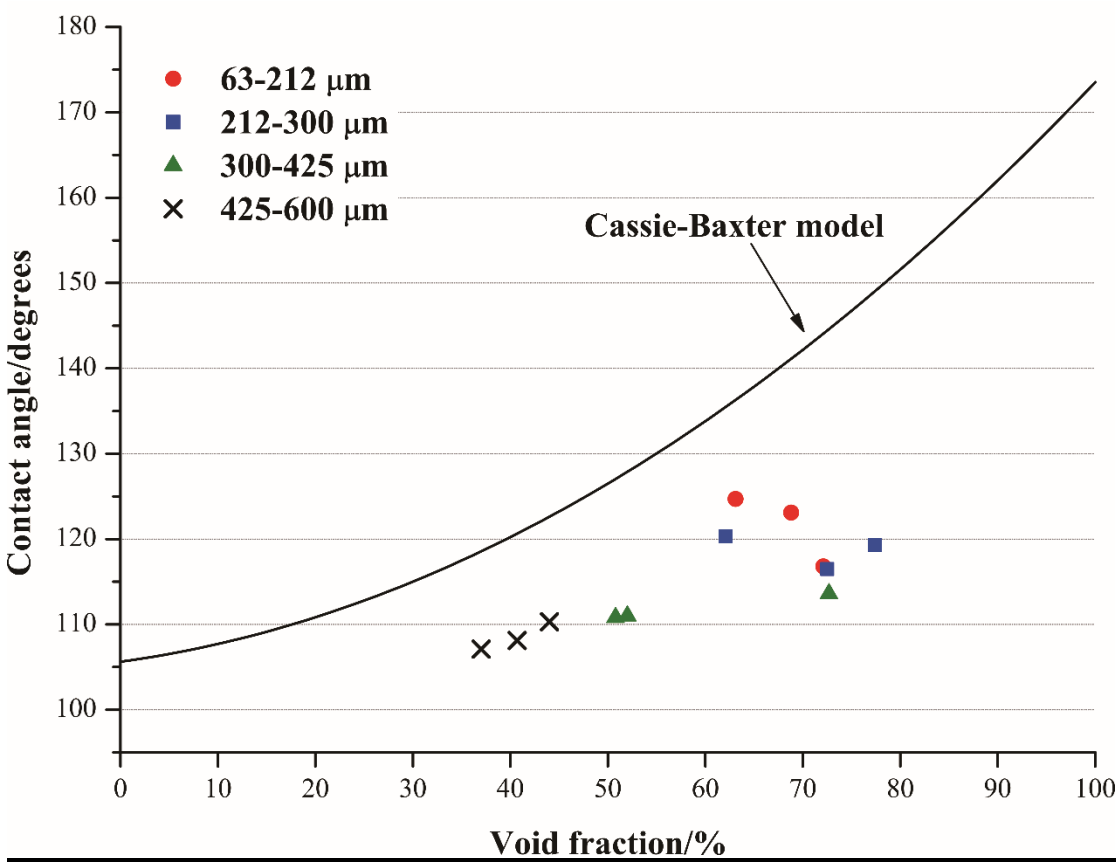

724

725 **Figure 9** Variation in void fraction with contact angle

726

727

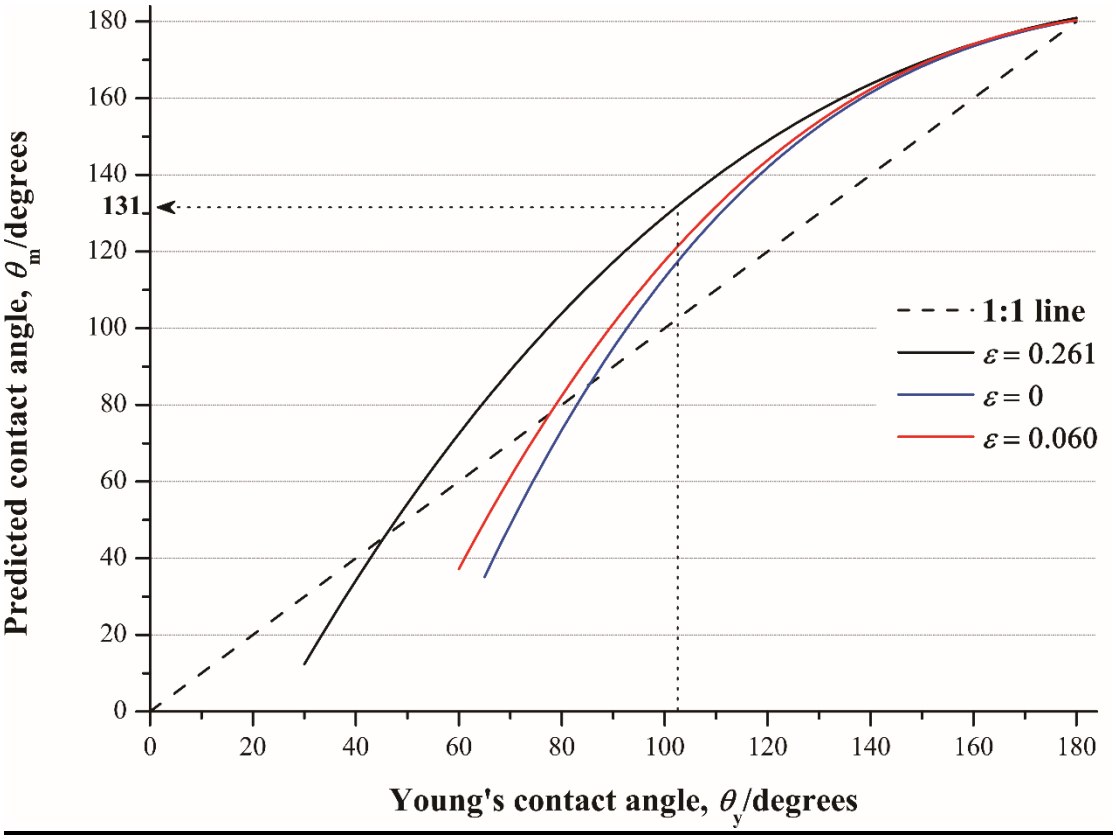

728

729 **Figure 10** Predicted contact angles according to model proposed by Bachmann &

730 McHale (2009) for the experimentally measured value of $\varepsilon = 0.261$ and fitted values

731 of $\varepsilon = 0$ and $\varepsilon = 0.060$

732

733